SANDIA REPORT
SAND2013-10619
Unlimited Release
Printed December 2013

Window Taper Functions for Subaperture Processing

Armin W. Doerry

Prepared by
Sandia National Laboratories
Albuquerque, New Mexico 87185 and Livermore, California 94550

Sandia National Laboratories is a multi-program laboratory managed and operated by Sandia Corporation, a wholly owned subsidiary of Lockheed Martin Corporation, for the U.S. Department of Energy's National Nuclear Security Administration under contract DE-AC04-94AL85000.

Sandia National Laboratories

Issued by Sandia National Laboratories, operated for the United States Department of Energy by Sandia Corporation.

Available to DOE and DOE contractors from

U.S. Department of Energy
Office of Scientific and Technical Information
P.O. Box 62
Oak Ridge, TN 37831

Telephone: (865) 576-8401
Facsimile: (865) 576-5728
E-Mail: reports@adonis.osti.gov
Online ordering: http://www.osti.gov/bridge

Available to the public from

U.S. Department of Commerce
National Technical Information Service
5285 Port Royal Rd.
Springfield, VA 22161

Telephone: (800) 553-6847
Facsimile: (703) 605-6900
E-Mail: orders@ntis.fedworld.gov
Online order: http://www.ntis.gov/help/ordermethods.asp?loc=7-4-0#online

SAND2013-10619
Unlimited Release
Printed December 2013

Window Taper Functions for Subaperture Processing

Armin W. Doerry
ISR Mission Engineering
Sandia National Laboratories
P.O. Box 5800
Albuquerque, NM 87185-0519

Abstract

It is well known that the spectrum of a signal can be calculated with a Discrete Fourier Transform (DFT), where best resolution is achieved by processing the entire data set. However, in some situations it is advantageous to use a staged approach, where data is first processed within subapertures, and the results are then combined and further processed to a final result. An artifact of this approach is the creation of grating lobes in the final response. The nature of the grating lobes, including their amplitude and spacing, is an artifact of window taper functions, subaperture offsets, and subaperture processing parameters. We assess these factors and exemplify their effects.

Acknowledgements

This report is the result of an unfunded Research and Development effort.

Sandia National Laboratories is a multi-program laboratory managed and operated by Sandia Corporation, a wholly owned subsidiary of Lockheed Martin Corporation, for the U.S. Department of Energy's National Nuclear Security Administration under contract DE-AC04-94AL85000.

Contents

Foreword

This report details the results of an academic study. It does not presently exemplify any modes, methodologies, or techniques employed by any operational system known to the author.

Classification

The specific mathematics and algorithms presented herein do not bear any release restrictions or distribution limitations.

This distribution limitations of this report are in accordance with the classification guidance detailed in the memorandum “Classification Guidance Recommendations for Sandia Radar Testbed Research and Development”, DRAFT memorandum from Brett Remund (Deputy Director, RF Remote Sensing Systems, Electronic Systems Center) to Randy Bell (US Department of Energy, NA-22), February 23, 2004. Sandia has adopted this guidance where otherwise none has been given.

This report formalizes preexisting informal notes and other documentation on the subject matter herein.

1 Introduction

Radar signal processing is essentially the implementation of a matched filter. Often, this matched filter is about matching to complex sinusoids. This often entails Fourier techniques to estimate time delay characteristics from spatial spectral content in the raw data. Central to this is the Discrete Fourier Transform (DFT), and its inverse. DFT processing is often 'nearly' the right processing technique, but not always quite 'exactly'.

It is often advantageous to implement the DFT (or its inverse) with subaperture techniques, allowing approximate phase error corrections to be implemented along the way, or facilitates reuse of partial processing results.

Several reports and papers discuss subaperture processing approaches to Synthetic Aperture Radar (SAR) processing.

> Burns and Cordaro[1] discuss the Overlapped Subaperture (OSA) SAR image formation technique. Cordaro elaborates on this technique in several limited-release reports. The aim here is to facilitate corrections to data characteristics not otherwise possible, or at least in a more efficient manner.
>
> Doerry[2,3,4] discusses multiple tiers of subapertures for SAR image formation in several reports and papers.
>
> Miller, et al.,[5] discuss subapertures applied to a VideoSAR processing algorithm. The aim here is to facilitate reuse of calculation results in multiple SAR images.

In this report, we address subaperture processing for Fourier analysis generically, unencumbered by needs of specific radar algorithms.

“You better cut the pizza in four pieces because I'm not hungry enough to eat six.”
-- Yogi Berra

2 Discussion

2.1 Sampled Complex Sinusoid

Consider a sampled function given by

$$x(n) = \exp(j\omega_0 n), \tag{1}$$

where

ω_0 = a constant phase-increment rate (frequency), and

$-\frac{N}{2} \le n < \frac{N}{2}$, where *n* is an integer that indicates sample index. (2)

For *n* outside this range, the function is zero.

A Discrete Fourier Transform (DFT) of function $x(n)$ over index *n* would yield

$$X(u) = \sum_{n=-N/2}^{N/2-1} x(n) \exp\left(-j2\pi \frac{u}{U} n\right), \tag{3}$$

where

$-\frac{U}{2} \le u < \frac{U}{2}$, where *u* is an integer. (4)

Typically, we have $U \ge N$. This is usually achieved by zero-padding the input data set.

We identify the transform pair as

$$X(u) \Leftrightarrow x(n). \tag{5}$$

We furthermore identify the function

$$\mathrm{csinc}_Z(z) = \frac{\sin \pi z}{\sin(\pi z/Z)} e^{-j\pi z/Z}. \tag{6}$$

Combining the previous results yields

$$X(u) = \mathrm{csinc}_N\left(\frac{N}{2\pi}\left(\omega_0 - \frac{2\pi}{U}u\right)\right). \tag{7}$$

We observe the following

- The DFT output $X(u)$ has a peak value of *N*.
- The DFT output $X(u)$ has a peak at output index value

$$u_0 = \frac{U}{2\pi}\omega_0 . \tag{8}$$

- The DFT output $X(u)$ has frequency spacing

$$\delta_u = \frac{2\pi}{U} . \tag{9}$$

- The DFT output $X(u)$ has nominal frequency resolution

$$\rho_u = \frac{2\pi}{N} . \tag{10}$$

- The DFT output $X(u)$ is periodic with period *U*. Therewith we may define values for $X(u)$ at index values *u* well outside the limits given in Eq. (4). That is, for integer *k*, we have

$$X(u) = X(u + kU) . \tag{11}$$

The output can then be written as

$$X(u) = \text{csinc}_N\left(\frac{\omega_0 - \delta_u u}{\rho_u}\right). \tag{12}$$

Note that we are sampling the spectrum of $x(n)$ at integer multiples of δ_u rad/sample. This is the result of using the DFT. That is

$$\omega_s(u) = \delta_u u \text{ = frequency samples.} \tag{13}$$

This allows us to write our result in terms of specific frequency sample positions as

$$X(u) = \text{csinc}_N\left(\frac{\omega_0 - \omega_s(u)}{\rho_u}\right). \tag{14}$$

Other or additional mechanisms would allow sampling the spectrum at other frequencies; not limited to the constraints of the DFT. These techniques might include interpolation, Chirp-Z Transform (CZT), or simple correlation. Nevertheless, we will continue our analysis assuming the DFT.

Nevertheless, our best estimate of the original signal's frequency is then calculated as

$$\hat{\omega}_0 = \omega_s\left(u_0\right) = \delta_u u_0 . \tag{15}$$

2.2 Subapertures

We now parse the input data set into subapertures, where

$$n = m_1 + \Delta_2 m_2 , \tag{16}$$

where

$$\begin{aligned} m_1 &= \text{intra-subaperture index with } -M_1/2 \le m_1 < M_1/2 , \\ m_2 &= \text{inter-subaperture index with } -M_2/2 \le m_2 < M_2/2 , \\ \Delta_2 &= \text{constant subaperture offset.} \end{aligned} \tag{17}$$

We note that

$$N = M_1 + \Delta_2 M_2 , \tag{18}$$

In general, the subapertures may overlap each other. Overlap will occur whenever

$$\Delta_2 < M_1 . \tag{19}$$

Typically, we select parameters such that even with overlap we have

$$\Delta_2 M_2 >> M_1 , \tag{20}$$

Nevertheless, the sampled sinusoid can now be written as a function of two indices as

$$x\left(n\right) = x\left(m_1, m_2\right) = \exp\left(j\omega_0 \left(m_1 + \Delta_2 m_2\right)\right) . \tag{21}$$

This can be separated as a product of independent functions as

$$x\left(m_1, m_2\right) = \exp\left(j\omega_0 m_1\right) \exp\left(j\omega_0 \Delta_2 m_2\right) . \tag{22}$$

With malice of forethought, we now also define the frequency index in terms of two new indices, namely

$$\frac{u}{U} = \frac{v_1}{V_1} + \frac{v_2}{\Delta_2 V_2}. \tag{23}$$

We expect that one index is perhaps a coarser spacing than the other. That is

$$V_1 \le \Delta_2 V_2. \tag{24}$$

We also typically desire that V_2 specifies the final frequency sample spacing, that is

$$\Delta_2 V_2 = U. \tag{25}$$

Consequently, we equate

$$\frac{u}{U} n = \left(\frac{v_1}{V_1} + \frac{v_2}{\Delta_2 V_2} \right) \left(m_1 + \Delta_2 m_2 \right). \tag{26}$$

The DFT now becomes the summation across both indices, namely

$$X\left(v_1, v_2\right) = \sum_{m_2 = -M_2/2}^{M_2/2} \left(\sum_{m_1 = -M_1/2}^{M_1/2} \left(\begin{array}{l} x\left(m_1, m_2\right) \\ \times \exp\left(-j2\pi \left(\frac{v_1}{V_1} + \frac{v_2}{\Delta_2 V_2} \right) \left(m_1 + \Delta_2 m_2 \right) \right) \end{array} \right) \right). \tag{27}$$

Applying this to our original signal results in

$$X\left(v_1, v_2\right) = \sum_{m_2 = -M_2/2}^{M_2/2} \left(\sum_{m_1 = -M_1/2}^{M_1/2} \left(\begin{array}{l} \exp\left(j\omega_0 \left(m_1 + \Delta_2 m_2 \right) \right) \\ \times \exp\left(-j2\pi \left(\frac{v_1}{V_1} + \frac{v_2}{\Delta_2 V_2} \right) \left(m_1 + \Delta_2 m_2 \right) \right) \end{array} \right) \right). \tag{28}$$

This can be parsed to

$$X\left(v_1,v_2\right)=\left(\begin{array}{l}\displaystyle\sum_{m_2=-M_2/2}^{M_2/2}\left(\begin{array}{l}\exp\left(j\omega_0\left(\Delta_2 m_2\right)\right)\\ \times\exp\left(-j2\pi\left(\dfrac{v_1}{V_1}+\dfrac{v_2}{\Delta_2 V_2}\right)\left(\Delta_2 m_2\right)\right)\end{array}\right)\\ \times\displaystyle\sum_{m_1=-M_1/2}^{M_1/2}\left(\begin{array}{l}\exp\left(j\omega_0 m_1\right)\\ \times\exp\left(-j2\pi\left(\dfrac{v_1}{V_1}+\dfrac{v_2}{\Delta_2 V_2}\right)m_1\right)\end{array}\right)\end{array}\right). \tag{29}$$

At this point for the summation over index m_1 we will make the approximation

$$\left(\frac{v_1}{V_1}+\frac{v_2}{\Delta_2 V_2}\right)\approx\frac{v_1}{V_1}. \tag{30}$$

This lets us approximate

$$X\left(v_1,v_2\right)\approx\left(\begin{array}{l}\displaystyle\sum_{m_2=-M_2/2}^{M_2/2}\left(\begin{array}{l}\exp\left(j\omega_0\left(\Delta_2 m_2\right)\right)\\ \times\exp\left(-j2\pi\left(\dfrac{v_1}{V_1}+\dfrac{v_2}{\Delta_2 V_2}\right)\left(\Delta_2 m_2\right)\right)\end{array}\right)\\ \times\displaystyle\sum_{m_1=-M_1/2}^{M_1/2}\left(\begin{array}{l}\exp\left(j\omega_0 m_1\right)\\ \times\exp\left(-j2\pi\left(\dfrac{v_1}{V_1}\right)m_1\right)\end{array}\right)\end{array}\right). \tag{31}$$

The summation over index m_1 now becomes a simple DFT with result

$$X\left(v_1,v_2\right)\approx\left(\begin{array}{l}\displaystyle\sum_{m_2=-M_2/2}^{M_2/2}\left(\begin{array}{l}\exp\left(j\omega_0\left(\Delta_2 m_2\right)\right)\\ \times\exp\left(-j2\pi\left(\dfrac{v_1}{V_1}+\dfrac{v_2}{\Delta_2 V_2}\right)\left(\Delta_2 m_2\right)\right)\end{array}\right)\\ \times\mathrm{csinc}_{M_1}\left(\dfrac{M_1}{2\pi}\left(\omega_0-\dfrac{2\pi}{V_1}v_1\right)\right)\end{array}\right). \tag{32}$$

The approximation of Eq. (30) for this result will be observable as a slight offset in the location of the csinc function. This will ultimately result in a frequency-dependent amplitude perturbation, or ripple, in the final result. More on this will be discussed later.

After this DFT we have a partial result where the data is in terms of indices m_2 and v_1. This partial result is described by the terms in the square brackets in the following rearranged equation

$$X\left(v_1,v_2\right)\approx\sum_{m_2=-M_2/2}^{M_2/2}\left(\begin{array}{l}\left[\operatorname{csinc}_{M_1}\left(\frac{M_1}{2\pi}\left(\omega_0-\frac{2\pi}{V_1}v_1\right)\right)\exp\left(j\omega_0\left(\Delta_2 m_2\right)\right)\right]\\ \times\exp\left(-j2\pi\left(\frac{v_1}{V_1}\right)\left(\Delta_2 m_2\right)\right)\\ \times\exp\left(-j2\pi\left(\frac{v_2}{V_2}\right)m_2\right)\end{array}\right). \quad (33)$$

However, if we multiply this interim data by the phase correction that is in fact described by the second exponential, we can associate terms as

$$X\left(v_1,v_2\right)\approx\sum_{m_2=-M_2/2}^{M_2/2}\left(\begin{array}{l}\left[\operatorname{csinc}_{M_1}\left(\frac{M_1}{2\pi}\left(\omega_0-\frac{2\pi}{V_1}v_1\right)\right)\exp\left(j\omega_0\left(\Delta_2 m_2\right)\right)\right]\\ \times\exp\left(-j2\pi\left(\frac{v_1}{V_1}\right)\left(\Delta_2 m_2\right)\right)\\ \times\exp\left(-j2\pi\left(\frac{v_2}{V_2}\right)m_2\right)\end{array}\right). \quad (34)$$

This phase correction is equivalent to shifting the original subaperture data prior to the transform, i.e. prepending zeroes corresponding to its position in the overall aperture. This accounts for a subaperture's position in the original data sequence. The square brackets now contain the corrected data. The summation over index m_2 now becomes a simple DFT of the entire function in the square brackets, which is our data appropriately corrected, with result

$$X\left(v_1,v_2\right)\approx\operatorname{csinc}_{M_1}\left(\frac{M_1}{2\pi}\left(\omega_0-\frac{2\pi}{V_1}v_1\right)\right)\operatorname{csinc}_{M_2}\left(\frac{M_2\Delta_2}{2\pi}\left(\omega_0-\frac{2\pi}{V_2\Delta_2}v_2-\frac{2\pi}{V_1}v_1\right)\right), \quad (35)$$

which can be written as

$$X\left(v_1,v_2\right)=\operatorname{csinc}_{M_1}\left(\frac{\omega_0-\delta_{v_1}v_1}{\rho_{v_1}}\right)\operatorname{csinc}_{M_2}\left(\frac{\omega_0-\delta_{v_2}v_2-\delta_{v_1}v_1}{\rho_{v_2}}\right). \quad (36)$$

where

$$\delta_{v_1} = \frac{2\pi}{V_1} \text{ = coarse-resolution output sample spacing,}$$

$$\rho_{v_1} = \frac{2\pi}{M_1} \text{ = coarse-resolution output nominal resolution,}$$

$$\delta_{v_2} = \frac{2\pi}{V_2 \Delta_2} \text{ = fine-resolution output sample spacing,}$$

$$\rho_{v_2} = \frac{2\pi}{M_2 \Delta_2} \text{ = fine-resolution output nominal resolution,}$$

V_1 = the zero-padded DFT length over index m_1, and

V_2 = the zero-padded DFT length over index m_2. (37)

Parameters are typically chosen such that

$$\rho_{v_2} << \rho_{v_1} \text{, and}$$

$$\delta_{v_2} << \delta_{v_1} . \quad (38)$$

A subtle point here is that since $M_2 \Delta_2 < N$ whenever we employ subapertures, there is a slight loss in achievable resolution in the final output spectrum.

Note that we are sampling the spectrum of our input signal at frequencies

$$\omega_s (v_1, v_2) = \delta_{v_1} v_1 + \delta_{v_2} v_2 \text{ = frequency samples.} \quad (39)$$

Returning to Eq. (36), we observe that it is a function of two index values. We may advantageously rewrite this in terms of a single frequency index as

$$X(u) = X(v_1, v_2) . \quad (40)$$

To relate these indices, we can manipulate the frequency sample locations such that

$$\omega_s (v_1, v_2) = \delta_{v_2} \left(\frac{\delta_{v_1}}{\delta_{v_2}} v_1 + v_2 \right). \quad (41)$$

We desire the single-index frequency sample locations to be

$$\omega_s (u) = \delta_{v_2} u \text{ = frequency samples.} \quad (42)$$

This implies that

$$u = \left(\frac{\delta_{v_1}}{\delta_{v_2}} v_1 + v_2 \right) = \left(\frac{V_2 \Delta_2}{V_1} v_1 + v_2 \right), \tag{43}$$

which is consistent with our earlier formulation. Note that generally more than one combination of legitimate index values for v_1 and v_2 will yield the same new single index value u, and in fact a peak in the second csinc function of Eq. (36). That is, for a particular single index value u, the specific index values for v_1 and v_2 are not unique. We solve this dilemma by choosing the index pair that yields the smallest value for $|v_2|$.

We note that a unit increment in index v_1 is equivalent to an increase in index v_2 of $\Delta_2 V_2 / V_1$. Consequently, we may limit our interest in values for v_2 to the range

$$-V_2^* / 2 \le v_2 < V_2^* / 2, \tag{44}$$

where

$$V_2^* = \frac{V_2 \Delta_2}{V_1} = \frac{\delta_{v_1}}{\delta_{v_2}}. \tag{45}$$

Some important observations include

- Eq. (36) is a product of two csinc functions, one each from DFT processing over the two indices m_1 and m_2. Each of these two sinc functions is a filter. The fine-resolution filter has better resolution than the coarse-resolution filter, but allows aliasing due to its sampling being decimated by offset factor Δ_2. The coarse-resolution filter resolves which of the aliased frequencies is the correct one.

- The 'needed' number of output samples V_2^* will always be less than or equal to the 'available' number of output samples V_2, and often far less.

- Under the right conditions, with coarse-resolution output sample spacing equal to the desired fine-resolution output sample spacing. i.e. when $\delta_{v_1} = \delta_{v_2}$, then we need only a single output sample from the fine-resolution DFT. That is, $V_2^* = 1$. In this case, the fine-resolution DFT may be replaced with a simple summation (which is equal to the calculation of the DC term).

- If we use strictly DFT calculations, then evenly spaced frequency sample locations $\omega_s(u)$ will require that $\Delta_2 V_2 / V_1$ reduces to an integer value. Otherwise we will need additional or more complicated processing.

This now allows us to create a single one-dimensional output vector where

$$X(u) = X(v_1, v_2) = \text{csinc}_{M_1}\left(\frac{\omega_0 - \delta_{v_1} v_1}{\rho_{v_1}}\right) \text{csinc}_{M_2}\left(\frac{\omega_0 - \delta_{v_2} v_2 - \delta_{v_1} v_1}{\rho_{v_2}}\right). \quad (46)$$

where the new single index relates to the original two indices as

$$u = \left(\frac{\delta_{v_1}}{\delta_{v_2}} v_1 + v_2\right) = \left(\frac{V_2 \Delta_2}{V_1} v_1 + v_2\right). \quad (47)$$

with the original indices constrained to

$$\begin{aligned} &-V_1/2 \le v_1 < V_1/2 \text{, and} \\ &-V_2^*/2 \le v_2 < V_2^*/2. \end{aligned} \quad (48)$$

We identify that the individual csinc functions will exhibit peaks at respective index values

$$\begin{aligned} &v_{1,0} = \omega_0/\delta_{v_1} \text{, and} \\ &v_{2,0} = \left(\omega_0 - \delta_{v_1} v_{1,0}\right)/\delta_{v_2}. \end{aligned} \quad (49)$$

To forestall any issue with aliasing, we specify the unique solution where

$$\begin{aligned} &-V_1/2 \le v_{1,0} < V_1/2 \text{, and} \\ &-V_2^*/2 \le v_{2,0} < V_2^*/2. \end{aligned} \quad (50)$$

Our best estimate of the input signal's frequency is then

$$\hat{\omega}_0 = \omega_s\left(v_{1,0}, v_{2,0}\right) = \delta_{v_1} v_{1,0} + \delta_{v_2} v_{2,0}. \quad (51)$$

Amplitude Correction

The approximation of Eq. (30) means any frequency that falls between output samples v_1 will be attenuated (and phase-adjusted) by the coarse-resolution csinc function. This attenuation function is given as relative to the center of the csinc function as

$$a(u) = a(v_1, v_2) = \frac{1}{M_1} \text{csinc}_{M_1}\left(\frac{\delta_{v_2} v_2}{\rho_{v_1}}\right). \quad (52)$$

This allows us to correct the output vector by calculating

$$X'(u) = X'(v_1, v_2) = \frac{X(v_1, v_2)}{a(v_1, v_2)}. \tag{53}$$

More explicitly, this can be expanded to

$$X'(u) = \frac{\text{csinc}_{M_1}\left(\frac{\omega_0 - \delta_{v_1} v_1}{\rho_{v_1}}\right)}{\frac{1}{M_1}\text{csinc}_{M_1}\left(\frac{\delta_{v_2} v_2}{\rho_{v_1}}\right)} \text{csinc}_{M_2}\left(\frac{\omega_0 - \delta_{v_2} v_2 - \delta_{v_1} v_1}{\rho_{v_2}}\right). \tag{54}$$

<u>Examples – Discussion</u>

We now illustrate some concepts with the following several examples.

Example 1 divides the data into non-overlapping subapertures. The input signal is a complex sinusoid with 0 cycles per vector, or DC. The spectrum shows a peak with sinc-like characteristics at 0 cycles per vector. It falls off to a zero amplitude at the edge of a coarse-resolution bin, at $\pm V_2^* / 2$. We like this.

Example 2 has all the same parameters as Example 1, except that the complex sinusoid now has frequency of 10 cycles per vector. The mainlobe still has the main peak at the proper frequency and still exhibiting a sinc-like characteristic, albeit not centered in a coarse-resolution bin anymore. However, note the strong grating lobes that have arisen. These are in fact aliased mainlobes that are not sufficiently attenuated by the coarse-resolution csinc function. The grating lobes do attenuate with distance from the mainlobe. Nevertheless, we don't like this.

Example 3 has the same parameters as Example 2 except that the subapertures have been overlapped by 50% resulting in an approximate doubling of the number of subapertures. The mainlobe still exhibits the same characteristic as before, but the grating lobes have slid farther away from the mainlobe by a factor of 2. Consequently, the tallest grating lobes have been reduced in amplitude. More overlap of the subapertures will push the grating lobes even farther away and reduce their levels even more. We like this better than the previous example.

Example 4 has the same parameters as Example 2 except that the coarse-resolution transform output has the same bin spacing as the final desired vector. This means that the fine-resolution transform is a simple summation of the processed subaperture outputs. Note that the output is a perfect csinc function without any grating lobes. This simply illustrates the linearity property of the DFT. We like this. We will address this case more fully later.

Example 1

Consider subaperture processing with the following parameters

$$\begin{aligned}
&\omega_0 = 0, \\
&M_1 = 64, \text{ processed with uniform weighting,} \\
&\Delta_2 = M_1 = 64, \text{ for non-overlapped subapertures,} \\
&M_2 = 16, \text{ processed with uniform weighting,} \\
&V_1 = M_1 = 64, \\
&V_2 = 12M_2 = 192.
\end{aligned} \tag{55}$$

In this case,

$$\begin{aligned}
&N = 1024, \\
&V_2^* = 192.
\end{aligned} \tag{56}$$

The assembled one-dimensional amplitude-corrected output vector $X'(u)$ is plotted in Figure 1.

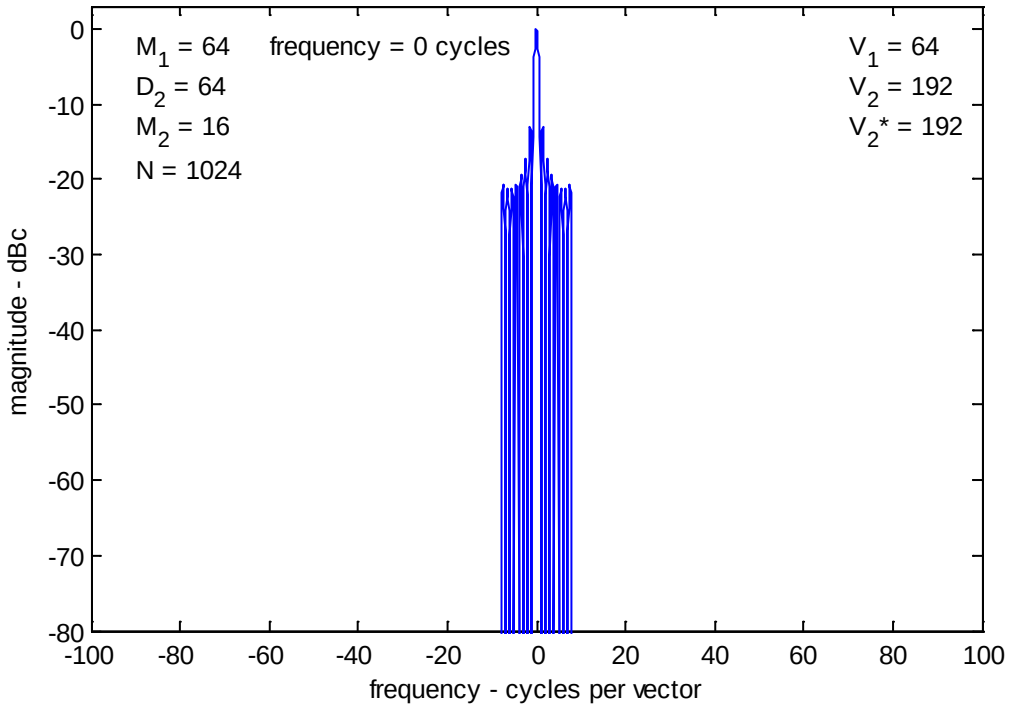

Figure 1. Spectral response for uniformly weighted data and non-overlapping subapertures.

Example 2

Consider subaperture processing with the following parameters

$$\begin{aligned}
&\omega_0 = 2\pi\ 10, \\
&M_1 = 64, \text{ processed with uniform weighting,} \\
&\Delta_2 = M_1 = 64, \text{ for non-overlapped subapertures,} \\
&M_2 = 16, \text{ processed with uniform weighting,} \\
&V_1 = M_1 = 64, \\
&V_2 = 12M_2 = 192.
\end{aligned} \tag{57}$$

In this case,

$$\begin{aligned}
&N = 1024, \\
&V_2^* = 192.
\end{aligned} \tag{58}$$

The assembled one-dimensional amplitude-corrected output vector $X'(u)$ is plotted in Figure 2.

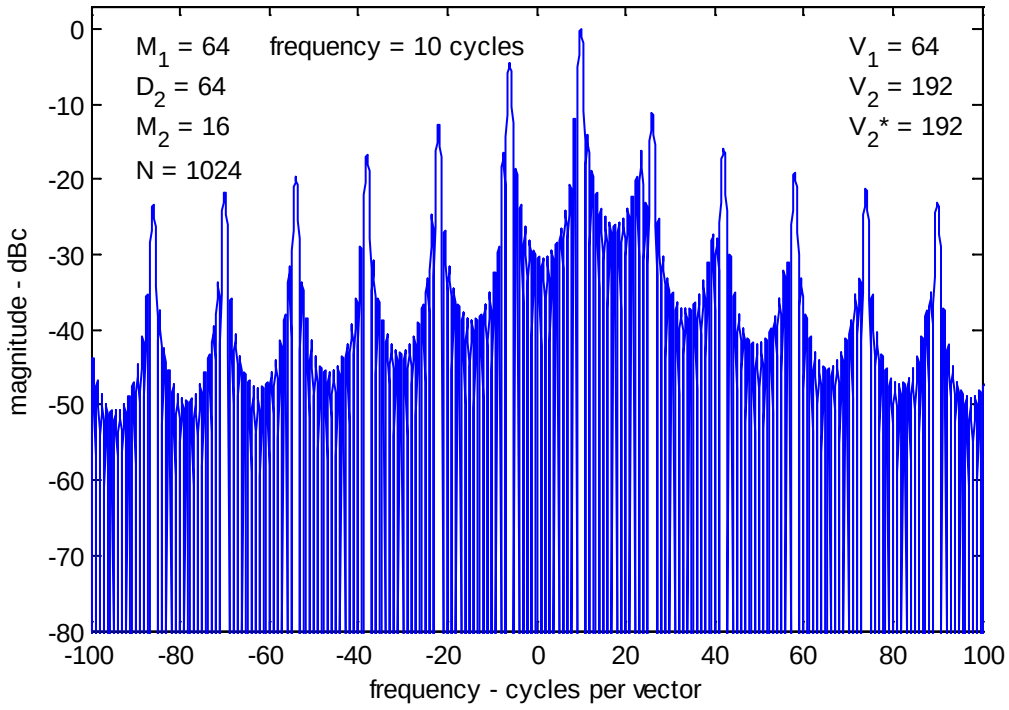

Figure 2. Spectral response for uniformly weighted data and non-overlapping subapertures.

Example 3

Consider subaperture processing with the following parameters

$$\begin{aligned}
&\omega_0 = 2\pi\ 10, \\
&M_1 = 64, \text{ processed with uniform weighting,} \\
&\Delta_2 = 32, \text{ for 50\% overlapped subapertures,} \\
&M_2 = 31, \text{ processed with uniform weighting,} \\
&V_1 = M_1 = 64, \\
&V_2 = 384.
\end{aligned} \tag{59}$$

In this case,

$$\begin{aligned}
&N = 1024, \\
&V_2^* = 192.
\end{aligned} \tag{60}$$

The assembled one-dimensional amplitude-corrected output vector $X'(u)$ is plotted in Figure 3.

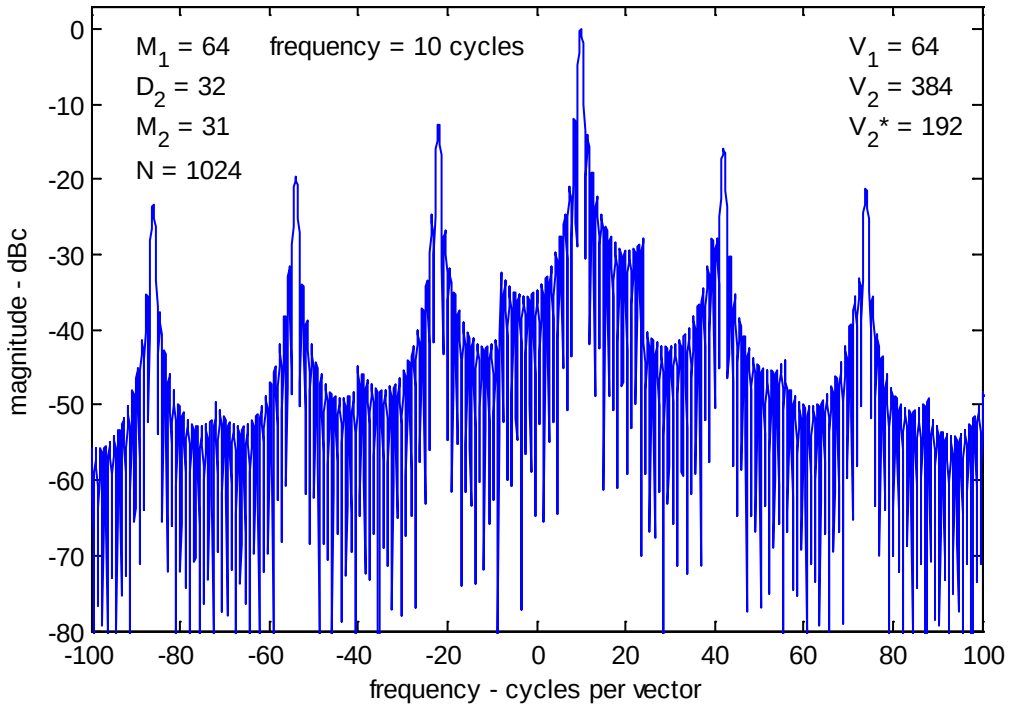

Figure 3. Spectral response for uniformly weighted data and overlapped subapertures.

Example 4

Consider subaperture processing with the following parameters

$$\begin{aligned}
&\omega_0 = 2\pi\ 10, \\
&M_1 = 64, \text{ processed with uniform weighting,} \\
&\Delta_2 = 64, \text{ for non-overlapped subapertures,} \\
&M_2 = 16, \text{ processed with uniform weighting,} \\
&V_1 = 12288, \\
&V_2 = 192.
\end{aligned} \tag{61}$$

In this case,

$$\begin{aligned}
&N = 1024, \\
&V_2^* = 1.
\end{aligned} \tag{62}$$

The assembled one-dimensional amplitude-corrected output vector $X'(u)$ is plotted in Figure 4.

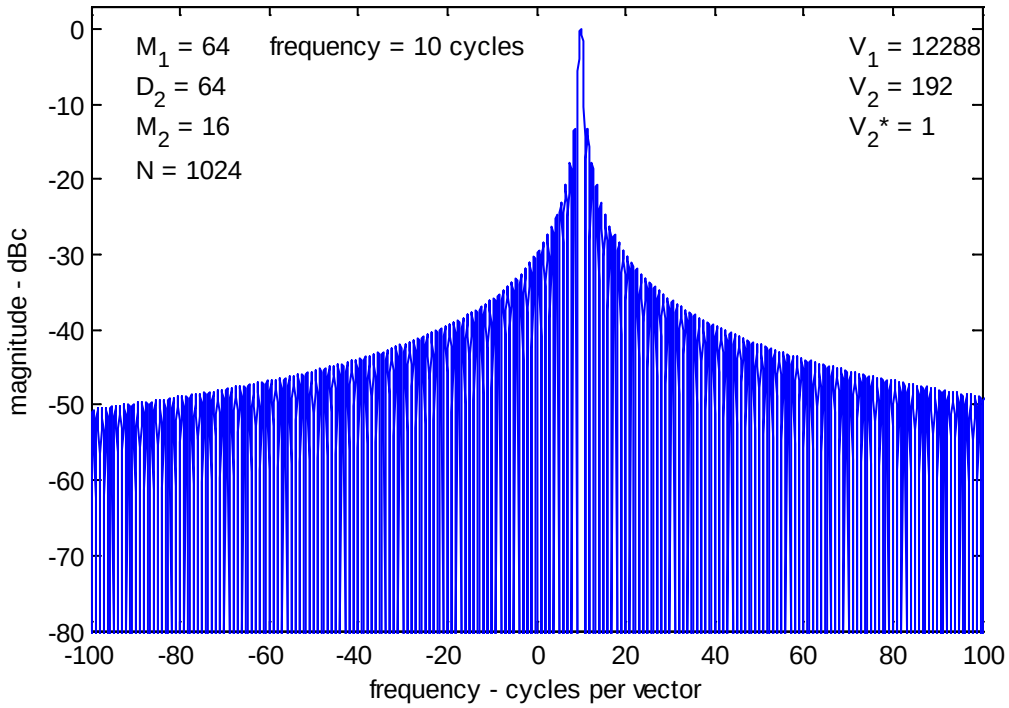

Figure 4. Spectral response for uniformly weighted data and non-overlapped subapertures, and subaperture output bin spacing equal to final bin spacing.

2.3 Subapertures with Windowed Data

Heretofore we have assumed no windowing or other sidelobe-control filtering prior to the coarse-resolution or the fine-resolution transforms. Consequently our frequency response has had a csinc-like mainlobe response with attendant relatively high sidelobes.

We now explore using window taper functions for sidelobe control in both the coarse-resolution transform and in the fine-resolution transform.

We return to Eq. (31) in the previous section, which is the processing model just prior to the first (coarse resolution) transform. However, we rewrite this equation and explicitly incorporate window functions as

$$X\left(v_1, v_2\right) \approx \left(\begin{array}{l} \displaystyle\sum_{m_2=-M_2/2}^{M_2/2} w_2\left(m_2\right) \left(\begin{array}{l} \exp\left(j\omega_0\left(\Delta_2 m_2\right)\right) \\ \times \exp\left(-j2\pi\left(\dfrac{v_1}{V_1} + \dfrac{v_2}{\Delta_2 V_2}\right)\left(\Delta_2 m_2\right)\right) \end{array} \right) \\ \times \displaystyle\sum_{m_1=-M_1/2}^{M_1/2} w_1\left(m_1\right) \left(\begin{array}{l} \exp\left(j\omega_0 m_1\right) \\ \times \exp\left(-j2\pi\left(\dfrac{v_1}{V_1}\right) m_1\right) \end{array} \right) \end{array} \right), \tag{63}$$

where the window functions are defined as

$$\begin{aligned} &w_1\left(m_1\right) \text{ = window function for coarse-resolution transform, and} \\ &w_2\left(m_2\right) \text{ = window function for fine-resolution transform.} \end{aligned} \tag{64}$$

Window functions are real-valued and even, and scaled such that

$$\begin{aligned} &\sum_{m_1=-M_1/2}^{M_1/2} w_1\left(m_1\right) = M_1, \text{ and} \\ &\sum_{m_2=-M_2/2}^{M_2/2} w_2\left(m_2\right) = M_2 . \end{aligned} \tag{65}$$

These window functions have DFTs that we specify as

$$\begin{aligned} &w_1\left(m_1\right) \Leftrightarrow W_{1,M_1}\left(\frac{M_1}{V_1 a_{w1}} v_1 \right), \text{ and} \\ &w_2\left(m_2\right) \Leftrightarrow W_{2,M_2}\left(\frac{M_2}{V_2 a_{w2}} v_2 \right), \end{aligned} \tag{66}$$

where we define the constants

$$a_{w1} = \text{mainlobe broadening factor for } w_1(m_1), \text{ and}$$
$$a_{w2} = \text{mainlobe broadening factor for } w_2(m_2). \tag{67}$$

The summation over index m_1 now becomes a simple DFT with result

$$X(v_1, v_2) \approx \sum_{m_2=-M_2/2}^{M_2/2} \left(\begin{bmatrix} W_{1,M_1}\left(\dfrac{\omega_0 - \delta_{v_1} v_1}{\rho_{v_1}} \right) \\ \times \exp\left(j\omega_0 (\Delta_2 m_2) \right) \\ \times \exp\left(-j2\pi \left(\dfrac{v_1}{V_1} \right) (\Delta_2 m_2) \right) \end{bmatrix} \times w_2(m_2) \exp\left(-j2\pi \left(\frac{v_2}{V_2} \right) (m_2) \right) \right), \tag{68}$$

where

$$\delta_{v_1} = \frac{2\pi}{V_1} = \text{coarse-resolution output sample spacing, and}$$
$$\rho_{v_1} = a_{w1} \frac{2\pi}{M_1} = \text{coarse-resolution output nominal resolution.} \tag{69}$$

The square brackets now contain the corrected data. The summation over index m_2 now becomes a simple DFT of the entire function in the square brackets but with the appropriate window function applied, which is our data appropriately corrected, with result

$$X(v_1, v_2) = W_{1,M_1}\left(\frac{\omega_0 - \delta_{v_1} v_1}{\rho_{v_1}} \right) W_{2,M_2}\left(\frac{\omega_0 - \delta_{v_2} v_2 - \delta_{v_1} v_1}{\rho_{v_2}} \right), \tag{70}$$

where

$$\delta_{v_2} = \frac{2\pi}{V_2 \Delta_2} = \text{fine-resolution output sample spacing,}$$
$$\rho_{v_2} = a_{w2} \frac{2\pi}{M_2 \Delta_2} = \text{fine-resolution output nominal resolution,} \tag{71}$$

Amplitude Correction

The approximation of Eq. (70) means any frequency that falls between output samples v_1 will be attenuated (and phase-adjusted) by the DFT of the coarse-resolution window function. This attenuation function is given as relative to the center of the DFT of the coarse-resolution function as

$$a(u) = a(v_1, v_2) = \frac{1}{M_1} W_{1,M_1}\left(\frac{\delta_{v_2} v_2}{\rho_{v_1}}\right). \tag{72}$$

This allows us to as before correct the output vector by calculating

$$X'(u) = X'(v_1, v_2) = \frac{X(v_1, v_2)}{a(v_1, v_2)}. \tag{73}$$

Examples – Discussion

We now build on the discussion of examples from the previous section.

Example 5 has subapertures overlapped by 50%, much like Example 3, except that the signal frequency has been returned to zero (DC), and window taper functions were employed during coarse-resolution processing and fine-resolution processing. Note that the mainlobe has its near-in sidelobes appropriately reduced as desired, but the frequency response departs from ideal at the coarse-resolution bin boundaries. Grating lobes are evident, but the tallest are nearly 40 dB down from the mainlobe peak.

Example 6 has its subapertures overlapped by 62.5%, which causes the grating lobes to slide farther away from the mainlobe, as expected. This also suppresses the tallest grating lobes to approximately 50 dB down from the mainlobe peak.

Example 7 has the same processing configuration as Example 6, but now operates on a complex sinusoid signal with a frequency of 10 cycles per input vector. Note that the mainlobe is very near a coarse-resolution bin boundary. Furthermore, note that both near-in sidelobes and grating lobes are no longer symmetric, and some grating lobes are in fact elevated from the DC frequency case.

Example 5

Consider subaperture processing with the following parameters

$$\begin{aligned}
&\omega_0 = 0,\\
&M_1 = 64, \text{ processed with } -50 \text{ dB Taylor window } (\bar{n} = 7),\\
&\Delta_2 = 32, \text{ for 50\% overlapped subapertures,}\\
&M_2 = 31, \text{ processed with } -35 \text{ dB Taylor window } (\bar{n} = 4),\\
&V_1 = 64,\\
&V_2 = 384.
\end{aligned} \tag{74}$$

In this case,

$$\begin{aligned}
&N = 1024,\\
&V_2^* = 192.
\end{aligned} \tag{75}$$

The assembled one-dimensional amplitude-corrected output vector $X'(u)$ is plotted in Figure 5.

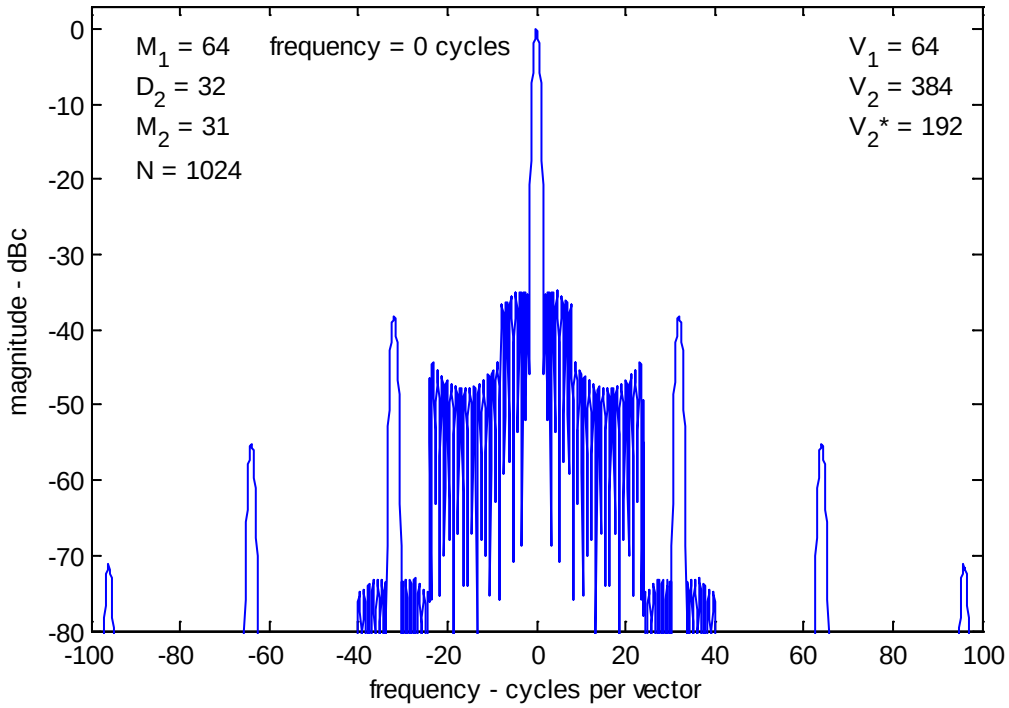

Figure 5. Spectral response for tapered data and overlapped subapertures.

Example 6

Consider subaperture processing with the following parameters

$$\begin{aligned}
&\omega_0 = 0,\\
&M_1 = 64, \text{ processed with } -50 \text{ dB Taylor window } (\bar{n} = 7),\\
&\Delta_2 = 24, \text{ for } 62.5\% \text{ overlapped subapertures,}\\
&M_2 = 41, \text{ processed with } -35 \text{ dB Taylor window } (\bar{n} = 4),\\
&V_1 = 64,\\
&V_2 = 512.
\end{aligned} \tag{76}$$

In this case,

$$\begin{aligned}
&N = 1024,\\
&V_2^* = 192.
\end{aligned} \tag{77}$$

The assembled one-dimensional amplitude-corrected output vector $X'(u)$ is plotted in Figure 6.

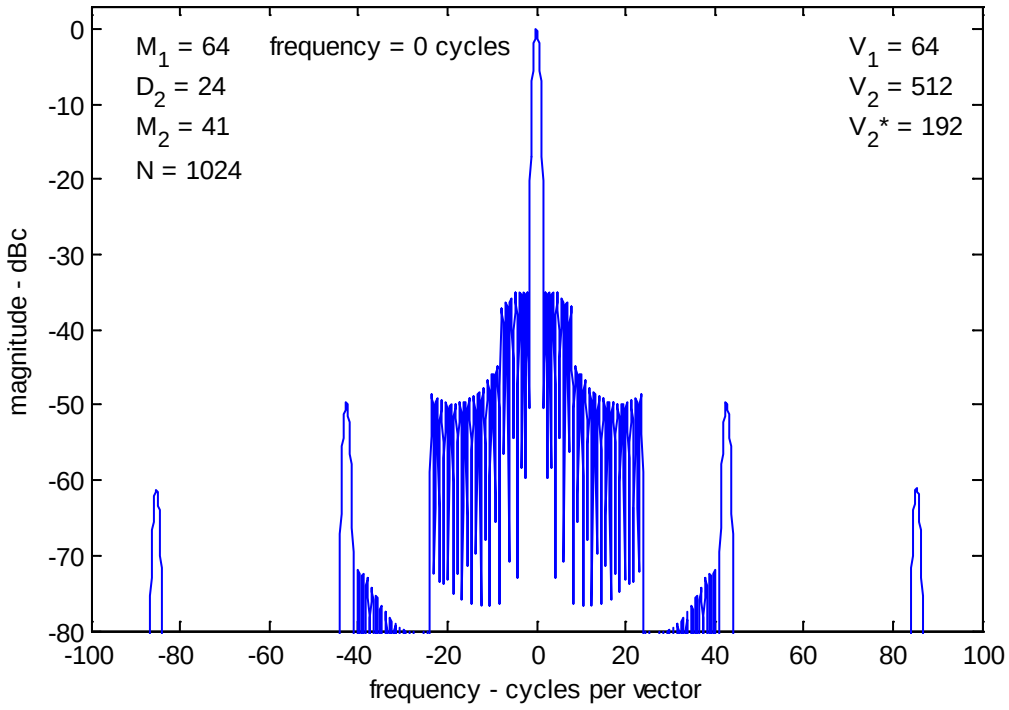

Figure 6. Spectral response for tapered data and overlapped subapertures.

Example 7

Consider subaperture processing with the following parameters

$$\begin{aligned}
&\omega_0 = 2\pi\ 10, \\
&M_1 = 64, \text{ processed with } -50 \text{ dB Taylor window } (\bar{n} = 7), \\
&\Delta_2 = 24, \text{ for } 62.5\% \text{ overlapped subapertures}, \\
&M_2 = 41, \text{ processed with } -35 \text{ dB Taylor window } (\bar{n} = 4), \\
&V_1 = 64, \\
&V_2 = 512.
\end{aligned} \tag{78}$$

In this case,

$$\begin{aligned}
&N = 1024, \\
&V_2^* = 192.
\end{aligned} \tag{79}$$

The assembled one-dimensional amplitude-corrected output vector $X'(u)$ is plotted in Figure 7.

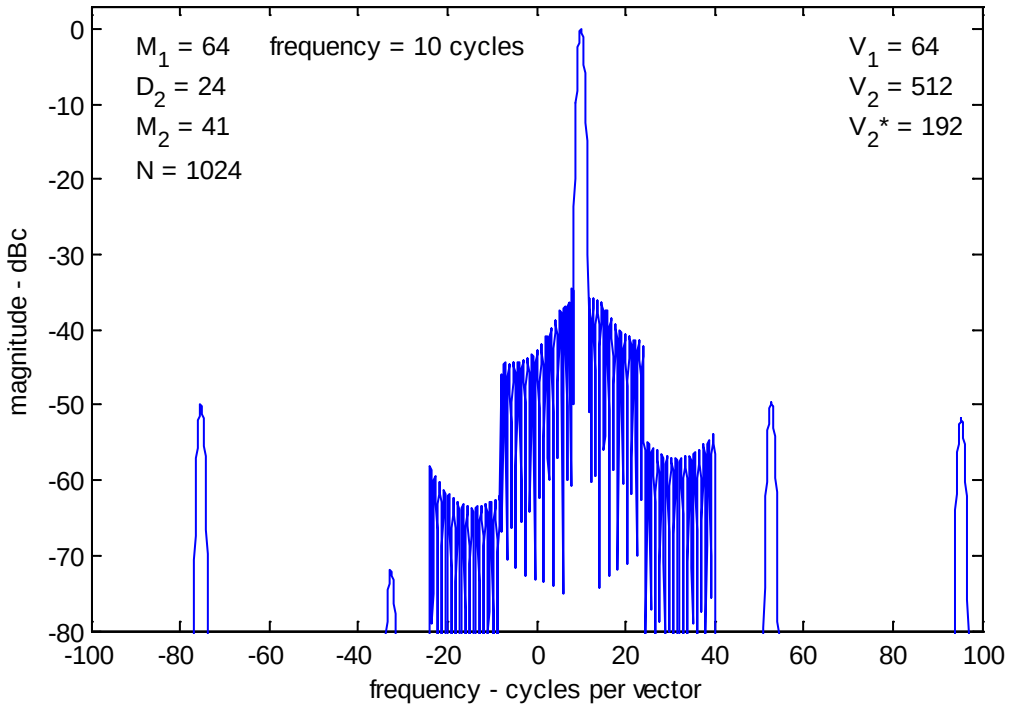

Figure 7. Spectral response for tapered data and overlapped subapertures.

2.4 Special Case – Subapertures Processed to Final Output Bin Spacing

We now examine the special case when the coarse-resolution processing produces output samples with the final desired bin spacing; the same as after fine-resolution processing. This is the case when

$$V_2^* = \frac{V_2 \Delta_2}{V_1} = \frac{\delta_{v_1}}{\delta_{v_2}} = 1. \tag{80}$$

In this case, the fine-resolution transform degenerates into a simple summation of the respective bins resulting from coarse-resolution processing.

Examples – Discussion

We now offer several examples to illustrate this special case.

Example 8 divides the data into non-overlapping subapertures, each processed with uniform window taper. The input signal is a complex sinusoid with 0 cycles per vector, or DC. The spectrum shows a mainlobe with near-in sidelobes with spectral characteristics consistent with the fine-resolution transform, which is simply a weighted summation in this case. Also obvious are the grating lobes centered at each coarse-resolution frequency bin. They are attenuated, but still exist at a relatively objectionable level.

Example 9 has all the same characteristics as Example 8 except that the subapertures are now processed with their own window taper function. The essential result is that near-in grating lobes are amplified, but far-out grating lobes are attenuated.

Example 10 uses subapertures overlapped by 50%, but otherwise keeps the same subaperture topology as Example 9. This causes the grating lobe spacing to double, thereby attenuating the grating lobes nearest to the mainlobe. This represents a significant improvement over Example 8.

Example 11 is identical to Example 10, with the exception that a different window taper function was employed for coarse-resolution subaperture processing. Note that a null has been placed on top of the grating lobe centers with sufficient null-width to essentially eliminate the grating lobes. Example 12 is the same processing as Example 11, except that the input signal has shifted frequency to 10 cycles per vector.

Example 13 uses the same input signal and processing as Example 11 except that a different yet window taper function was employed for coarse-resolution subaperture processing. Although an improvement over the results of Example 10, it still doesn't quite match the results of Example 11.

Example 8

Consider subaperture processing with the following parameters

$$\begin{aligned}
&\omega_0 = 0,\\
&M_1 = 64, \text{ processed with uniform taper,}\\
&\Delta_2 = 64, \text{ for non-overlapped subapertures,}\\
&M_2 = 16, \text{ processed with } -35 \text{ dB Taylor window } (\bar{n} = 4),\\
&V_1 = 12288,\\
&V_2 = 192.
\end{aligned} \tag{81}$$

In this case,

$$\begin{aligned}
&N = 1024,\\
&V_2^* = 1.
\end{aligned} \tag{82}$$

The assembled one-dimensional amplitude-corrected output vector $X'(u)$ is plotted in Figure 8.

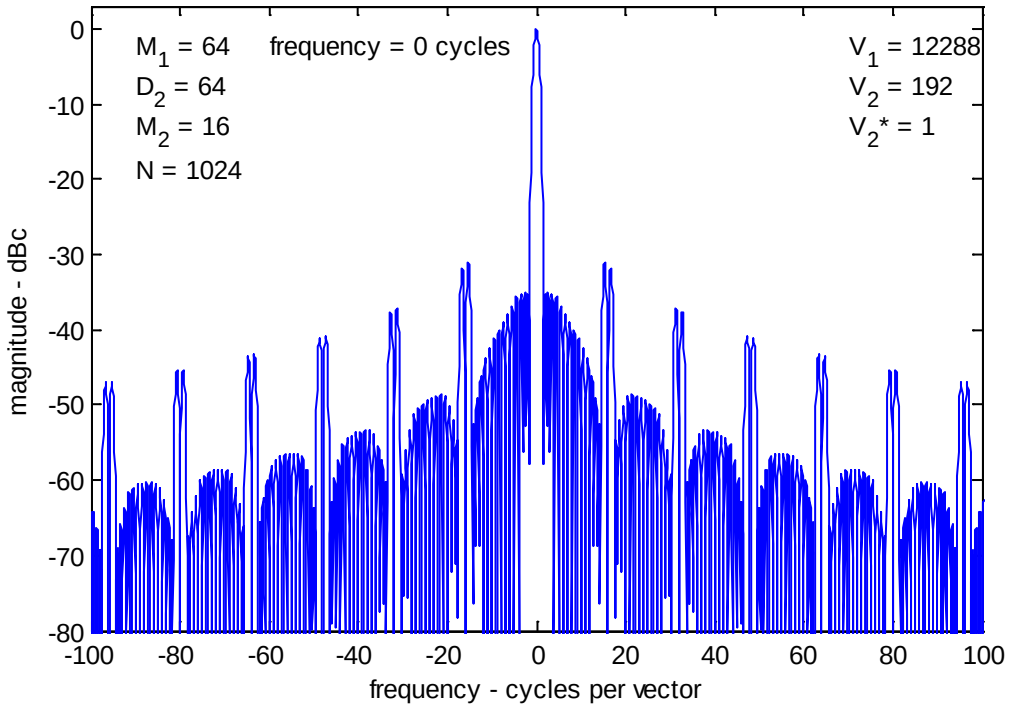

Figure 8. Spectral response for tapered data and non-overlapped subapertures.

Example 9

Consider subaperture processing with the following parameters

$$\begin{aligned}
&\omega_0 = 0,\\
&M_1 = 64, \text{ processed with } -50 \text{ dB Taylor window } (\bar{n} = 7),\\
&\Delta_2 = 64, \text{ for non-overlapped subapertures,}\\
&M_2 = 16, \text{ processed with } -35 \text{ dB Taylor window } (\bar{n} = 4),\\
&V_1 = 12288,\\
&V_2 = 192.
\end{aligned} \tag{83}$$

In this case,

$$\begin{aligned}
&N = 1024,\\
&V_2^* = 1.
\end{aligned} \tag{84}$$

The assembled one-dimensional amplitude-corrected output vector $X'(u)$ is plotted in Figure 9.

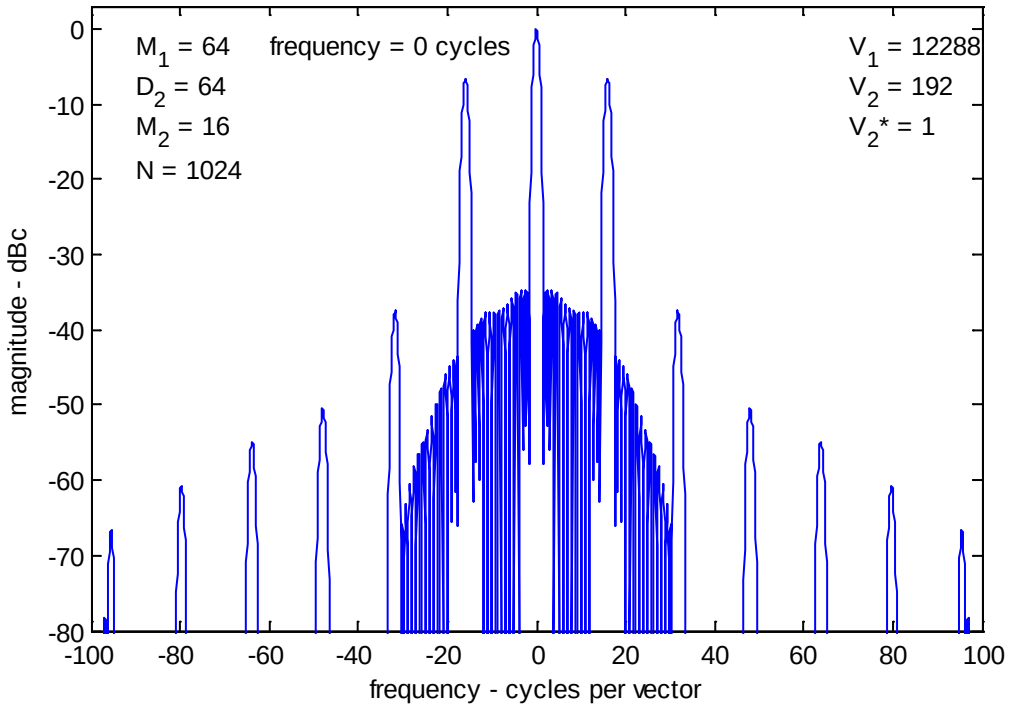

Figure 9. Spectral response for tapered data and non-overlapped subapertures.

Example 10

Consider subaperture processing with the following parameters

$$\begin{aligned}
&\omega_0 = 0,\\
&M_1 = 64, \text{ processed with } -50 \text{ dB Taylor window } (\bar{n} = 7),\\
&\Delta_2 = 32, \text{ for 50\% overlapped subapertures,}\\
&M_2 = 31, \text{ processed with } -35 \text{ dB Taylor window } (\bar{n} = 4),\\
&V_1 = 12288,\\
&V_2 = 384.
\end{aligned} \tag{85}$$

In this case,

$$\begin{aligned}
&N = 1024,\\
&V_2^* = 1.
\end{aligned} \tag{86}$$

The assembled one-dimensional amplitude-corrected output vector $X'(u)$ is plotted in Figure 10.

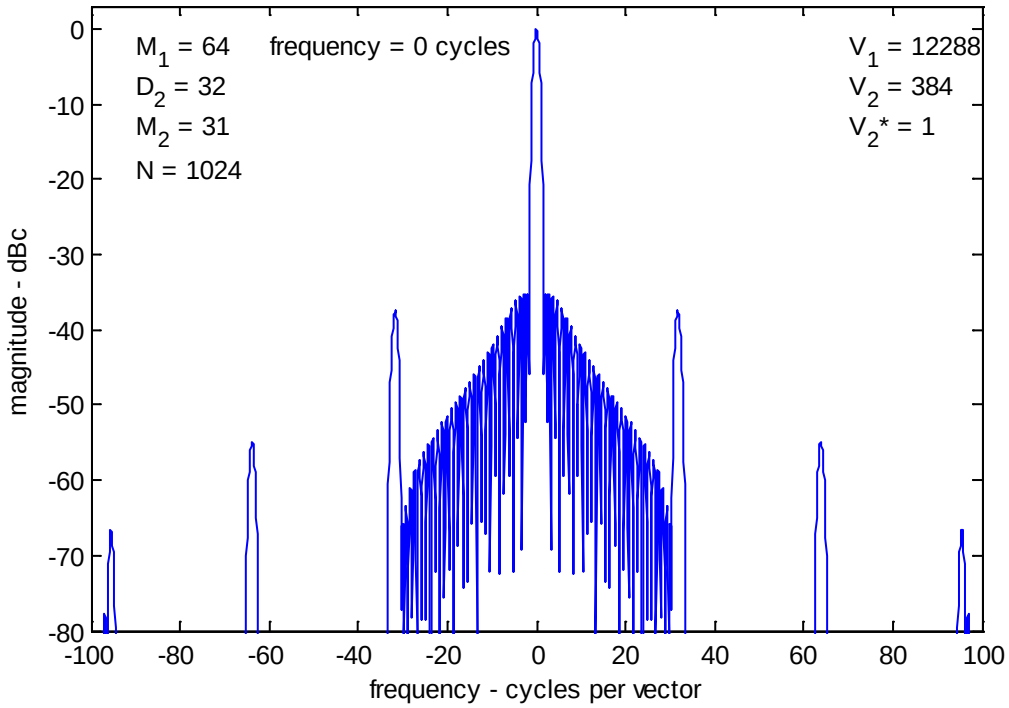

Figure 10. Spectral response for tapered data and overlapped subapertures.

Example 11

Consider subaperture processing with the following parameters

$$\begin{aligned}
&\omega_0 = 0,\\
&M_1 = 64, \text{ processed with triangular window,}\\
&\Delta_2 = 32, \text{ for 50\% overlapped subapertures,}\\
&M_2 = 31, \text{ processed with } -35 \text{ dB Taylor window } (\bar{n} = 4),\\
&V_1 = 12288,\\
&V_2 = 384.
\end{aligned} \tag{87}$$

In this case,

$$\begin{aligned}
&N = 1024,\\
&V_2^* = 1.
\end{aligned} \tag{88}$$

The assembled one-dimensional amplitude-corrected output vector $X'(u)$ is plotted in Figure 11.

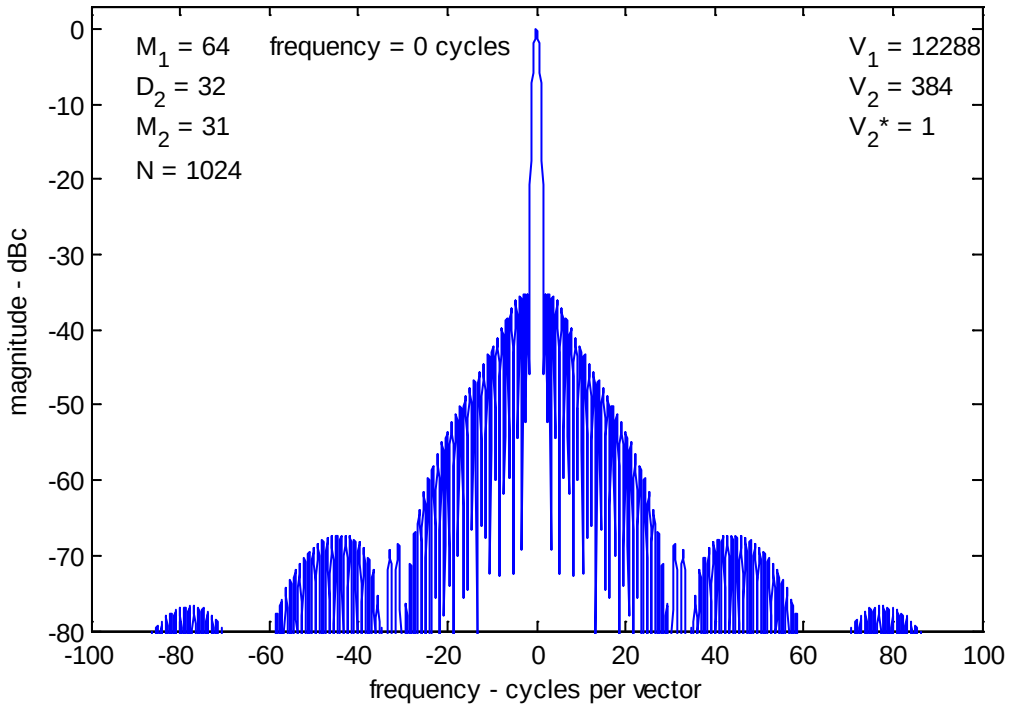

Figure 11. Spectral response for tapered data and overlapped subapertures.

Example 12

Consider subaperture processing with the following parameters

$$\begin{aligned}
&\omega_0 = 2\pi\, 10, \\
&M_1 = 64, \text{ processed with triangular window,} \\
&\Delta_2 = 32, \text{ for 50\% overlapped subapertures,} \\
&M_2 = 31, \text{ processed with } -35 \text{ dB Taylor window } (\bar{n} = 4), \\
&V_1 = 12288, \\
&V_2 = 384.
\end{aligned} \tag{89}$$

In this case,

$$\begin{aligned}
&N = 1024, \\
&V_2^* = 1.
\end{aligned} \tag{90}$$

The assembled one-dimensional amplitude-corrected output vector $X'(u)$ is plotted in Figure 12.

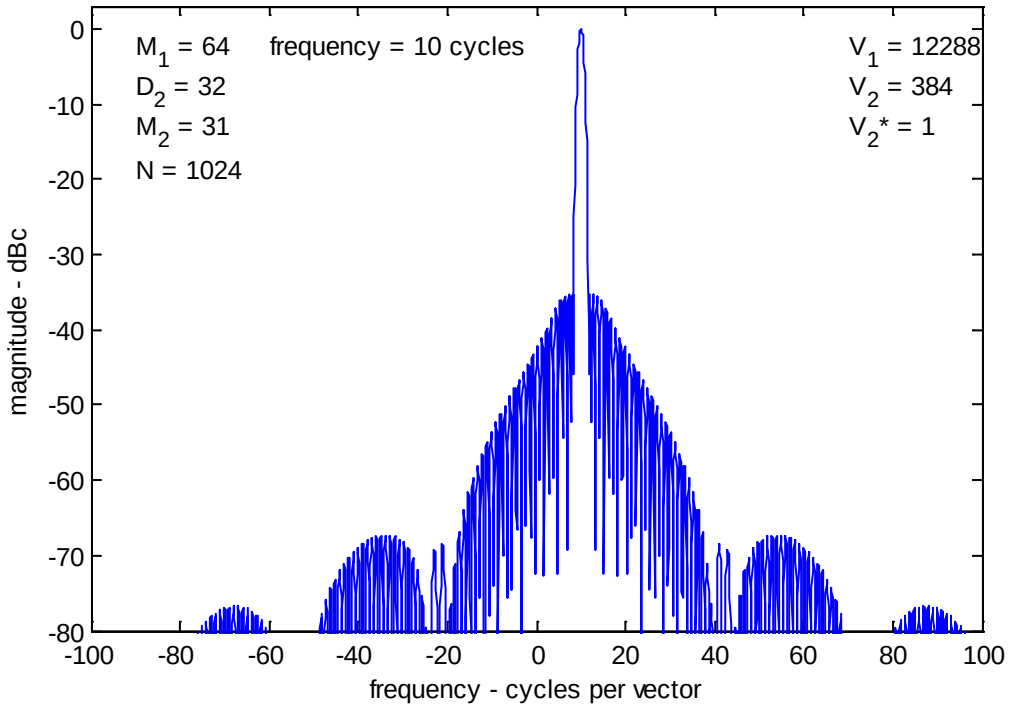

Figure 12. Spectral response for tapered data and overlapped subapertures.

Example 13

Consider subaperture processing with the following parameters

$$\begin{aligned}
&\omega_0 = 0,\\
&M_1 = 64, \text{ processed with raised cosine window,}\\
&\Delta_2 = 32, \text{ for 50\% overlapped subapertures,}\\
&M_2 = 31, \text{ processed with } -35 \text{ dB Taylor window } (\bar{n} = 4),\\
&V_1 = 12288,\\
&V_2 = 384.
\end{aligned} \tag{91}$$

In this case,

$$\begin{aligned}
&N = 1024,\\
&V_2^* = 1.
\end{aligned} \tag{92}$$

The assembled one-dimensional amplitude-corrected output vector $X'(u)$ is plotted in Figure 13.

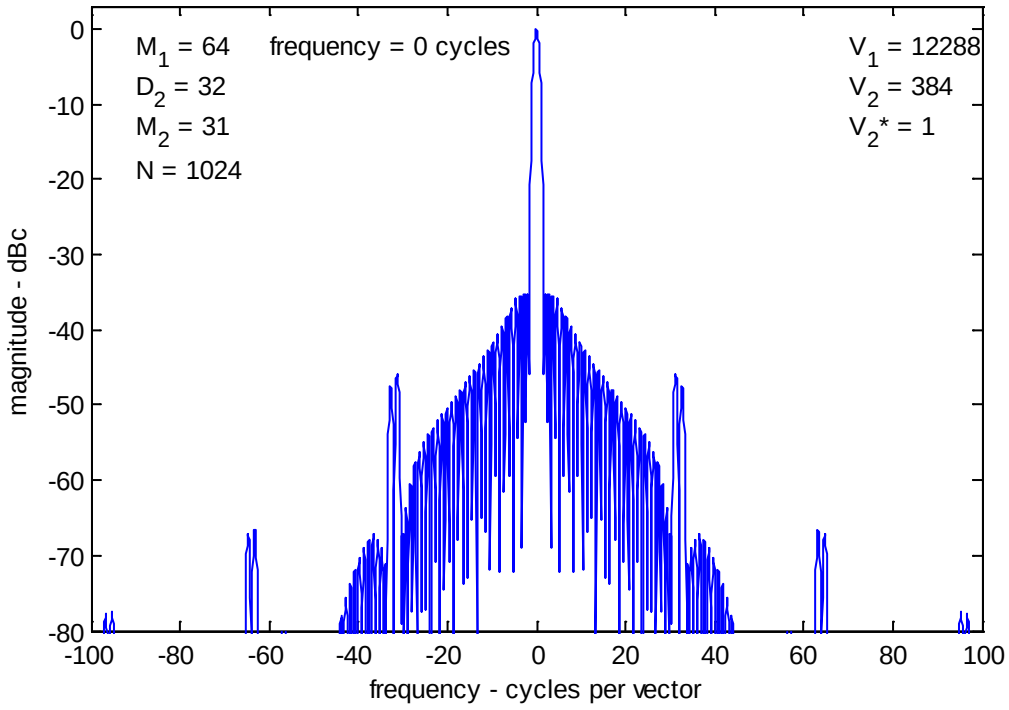

Figure 13. Spectral response for tapered data and overlapped subapertures.

Gratuitous Observations

It is interesting to plot the combined weighting factors for the input data.

Figure 14 illustrates the input data taper for Example 8. Note the 'chunky' nature of the summed subapertures. These discontinuities result in the high grating lobes in the final spectrum.

Figure 15 illustrates the input data taper for Example 11. The summed subapertures are considerably smoothed. In fact the summed subaperture curve is a series of linear segments. The smoothed nature of this curve is responsible for the grating lobe suppression.

Figure 16 illustrates the input data taper for Example 13. The summed subapertures are considerably smoothed compared to Figure 14, but not as smooth as in Figure 15; exhibiting some ripple. Consequently the grating lobes are less pronounced than for Example 8, but more pronounced than for Example 11.

The effects do depend somewhat on the fine-resolution window taper function. For example, had the fine-resolution window been uniform, then there would be essentially no difference in using the raised-cosine subaperture window over the triangle subaperture window, or for that matter using a uniform subaperture window.

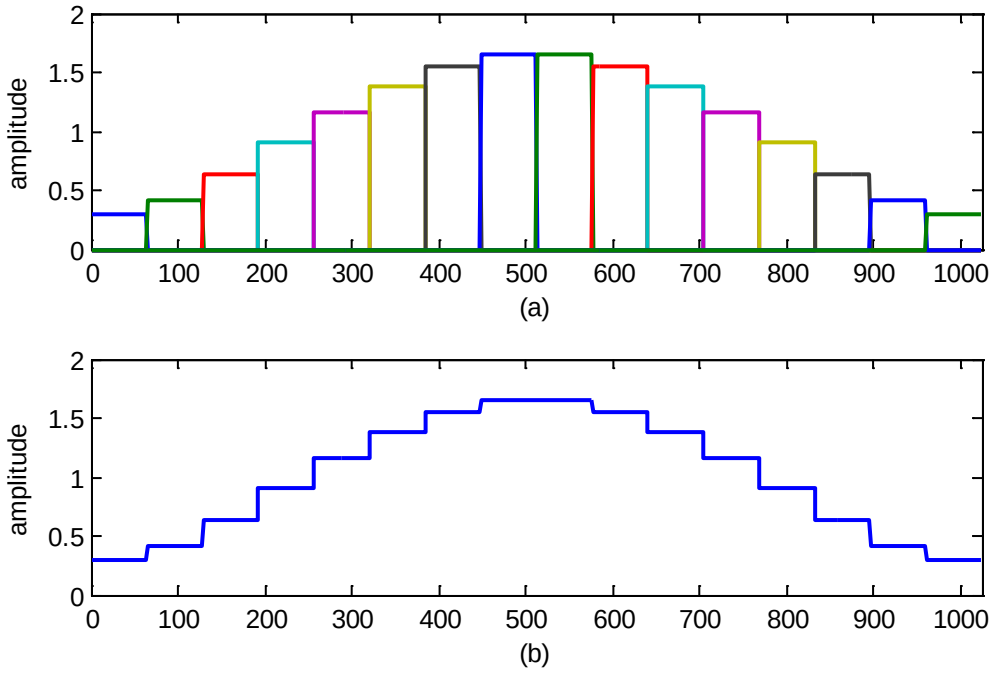

Figure 14. Input data taper for Example 8, including (a) the individual subapertures, and (b) the summation of the subapertures.

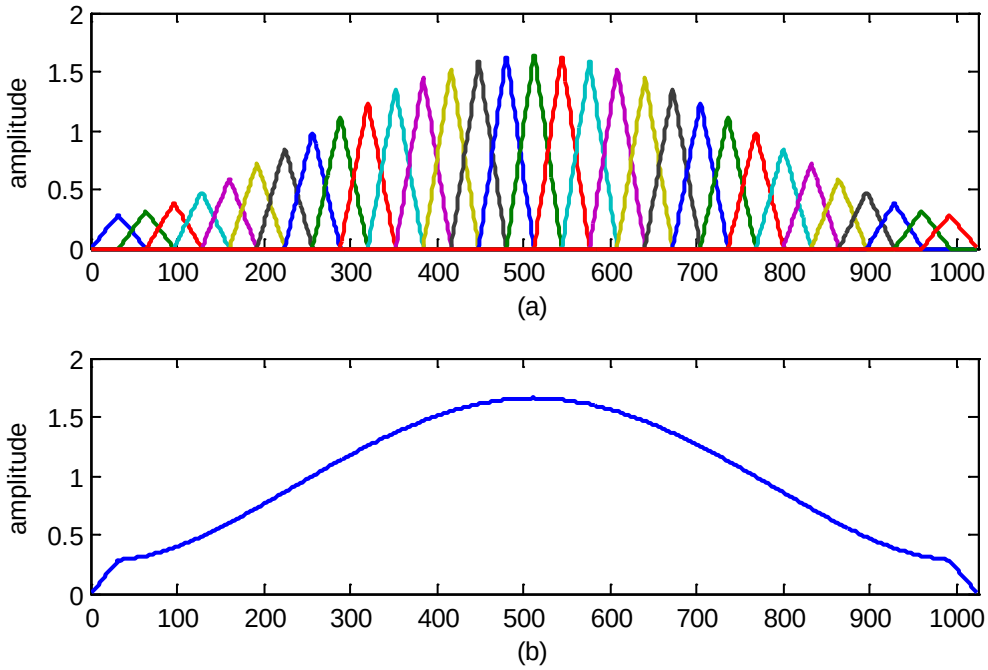

Figure 15. Input data taper for Example 11, including (a) the individual subapertures, and (b) the summation of the subapertures.

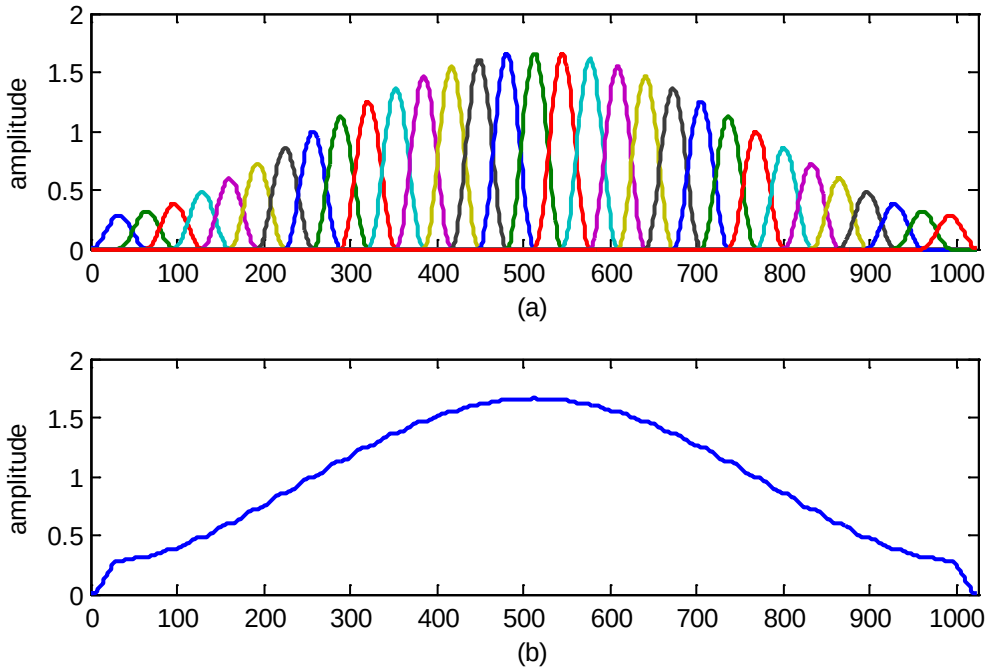

Figure 16. Input data taper for Example 13, including (a) the individual subapertures, and (b) the summation of the subapertures.

2.5 Subaperture Processing Algorithm

The steps to implement subaperture processing are detailed in Figure 17.

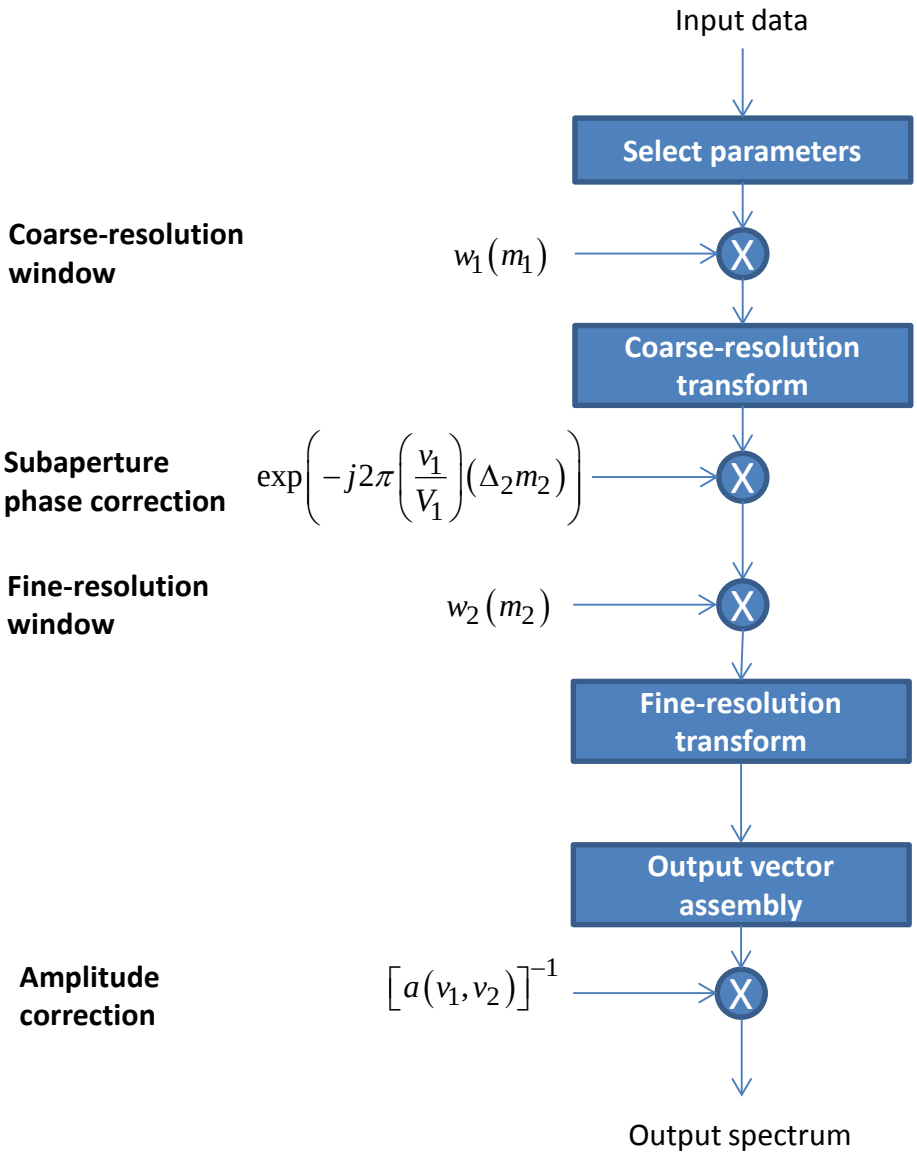

Figure 17. Processing flow diagram.

2.6 Miscellaneous Comments

We now offer a number of comments concerning various aspects of subaperture processing.

- The biggest issue with employing subapertures is that the output spectrum generally exhibits undesirable grating lobes. These grating lobes are in fact aliased mainlobe due to the decimation of the data rate inherent in the subaperture offsets.

- The fine-resolution window taper function determines near-in sidelobe response, whereas the coarse-resolution window taper function generally determines the nature of the grating lobes insofar as how fast they fall off in amplitude with distance from the mainlobe. The offset and overlap of the subapertures determines the spacing of the grating lobes.

- In some circumstances, the proper choice of coarse-resolution window taper function can substantially reduce the amplitude of the grating lobes by placing the grating lobes into deep nulls with sufficient null-width. This is especially true for the special case where the subapertures are processed to the final output bin spacing.

- There is an inherent worsening of achievable resolution in the output spectrum by a factor $N/(M_2\Delta_2)$. This is usually small, but very real. It can be compensated by collecting a longer input data vector with this in mind.

- Not explored herein, but nevertheless not out of the question, is the possibility of using different subaperture window taper functions for different subapertures. In fact, no explicit requirement exists to even maintain the same subaperture size, or a constant subaperture offset.

- The concept of subapertures was explored herein in the context of evaluating a signal's frequency spectrum. These concepts are quite applicable to multi-phase-center antennas as are commonly employed in high-performance Interferometric radar systems. Furthermore, the concepts herein can be extended to multi-dimensional apertures, including applications in image processing and in antenna systems.

“Arrange whatever pieces come your way.”
-- Virginia Woolf

3 Conclusions

We reiterate the following points and observations

- Subaperture processing turns a one-dimensional calculation into a two-dimensional calculation. More generally, each tier of subapertures increases the dimensionality of the processing by one. For many applications this yields some benefit, either in data reuse or mitigation of undesirable data characteristics.

- Results achieved using subapertures are in several respects not quite as good as a single transform across the entire data set, but in turn offer some unique advantages not otherwise possible.

- An artifact of subaperture processing is the generation of grating lobes, whose characteristics are dependent on window taper functions used on the subapertures and in final trans-subaperture processing, as well as the nature of the overlap in adjacent subapertures. Subaperture processing output bin spacing also plays a role.

- In addition to transforms on individual subapertures, and across the results of the multiple subapertures, proper processing also requires intermediate phase manipulation and final amplitude corrections.

"It is easier to achieve a desired result in short pieces."
-- Gustav Mahler

Appendix A – The csinc Function

Consider the exponential sequence

$$X = \sum_{n=-N/2}^{N/2-1} \exp\left(j2\pi\Omega n \right). \tag{93}$$

A change of index variable allows this to be written as

$$X = \sum_{m=0}^{N-1} \exp\left(j2\pi\Omega\left(m - N/2 \right) \right), \tag{94}$$

This can be separated and expanded to

$$X = \sum_{m=0}^{N-1} \exp\left(j2\pi\Omega m \right) \exp\left(j2\pi\Omega\left(-N/2 \right) \right), \tag{95}$$

and further to

$$X = \exp\left(j2\pi\Omega\left(-N/2 \right) \right) \left[\frac{1 - \exp\left(j2\pi\Omega N \right)}{1 - \exp\left(j2\pi\Omega \right)} \right]. \tag{96}$$

This can be factored to the expression

$$\begin{aligned} X = {} & \exp\left(j2\pi\Omega\left(-N/2 \right) \right) \frac{\exp\left(j2\pi\Omega \frac{N}{2} \right)}{\exp\left(j2\pi\Omega \frac{1}{2} \right)} \\ & \times \left[\frac{\exp\left(-j2\pi\Omega \frac{N}{2} \right) - \exp\left(j2\pi\Omega \frac{N}{2} \right)}{\exp\left(-j2\pi\Omega \frac{1}{2} \right) - \exp\left(j2\pi\Omega \frac{1}{2} \right)} \right] \end{aligned}, \tag{97}$$

and simplified to

$$X = \frac{1}{\exp\left(j2\pi\Omega \frac{1}{2} \right)} \left[\frac{\exp\left(-j2\pi\Omega \frac{N}{2} \right) - \exp\left(j2\pi\Omega \frac{N}{2} \right)}{\exp\left(-j2\pi\Omega \frac{1}{2} \right) - \exp\left(j2\pi\Omega \frac{1}{2} \right)} \right], \tag{98}$$

Using the Euler formula, we identify that this equates to

$$X = \exp\left(-j2\pi\Omega\frac{1}{2}\right)\frac{\sin\left(2\pi\Omega\frac{N}{2}\right)}{\sin\left(2\pi\Omega\frac{1}{2}\right)}, \tag{99}$$

which can be rearranged to

$$X = \frac{\sin\left(\pi\Omega N\right)}{\sin\left(\pi\Omega\right)}\exp\left(-j\pi\Omega\right). \tag{100}$$

For the moment we will equate

$$z = \Omega N, \tag{101}$$

which allows us to write

$$X = \frac{\sin\left(\pi z\right)}{\sin\left(\pi\frac{z}{N}\right)}\exp\left(-j\pi\frac{z}{N}\right), \tag{102}$$

which we in turn identify as

$$X = \mathrm{csinc}_N\left(z\right). \tag{103}$$

Consequently, we identify the closed-form solution to the exponential sequence as

$$\sum_{n=-N/2}^{N/2-1}\exp\left(j2\pi z\frac{n}{N}\right) = \mathrm{csinc}_N\left(z\right) = \frac{\sin\left(\pi z\right)}{\sin\left(\pi\frac{z}{N}\right)}\exp\left(-j\pi\frac{z}{N}\right). \tag{104}$$

References

[1] B. L. Burns, J. T. Cordaro, “SAR image formation algorithm that compensates for the spatially variant effects of antenna motion”, SPIE Proceedings, Vol 2230, SPIE’s International Symposium on Optical Engineering in Aerospace Sensing, Orlando, 4-8 April 1994.

[2] Armin W. Doerry, "Synthetic Aperture Radar Processing with Tiered Subapertures", Sandia Report SAND94-1390, June, 1994.

[3] A. W. Doerry, "Synthetic Aperture Radar Processing with Polar Formatted Subapertures", Conference Record of The Twenty-Eighth Asilomar Conference on Signals, Systems & Computers, Pacific Grove, California, Oct. 31 - Nov. 2, 1994, pp 1210-1215.

[4] Armin W. Doerry, "Synthetic Aperture Radar Processing with Tiered Subapertures", Ph.D. Dissertation, University of New Mexico, Albuquerque, New Mexico, May, 1995.

[5] J. Miller, E. Bishop, A. Doerry, “An Application of Backprojection for Video SAR Image Formation Exploiting a Subaperture Circular Shift Register”, SPIE 2013 Defense, Security & Sensing Symposium, Algorithms for Synthetic Aperture Radar Imagery XX, Vol. 8746, Baltimore MD, 29 April – 3 May 2013.

Distribution

Unlimited Release

1	MS 0519	J. A. Ruffner	5349	
1	MS 0519	A. W. Doerry	5349	
1	MS 0519	L. Klein	5349	
1	MS 0532	J. J. Hudgens	5240	
1	MS 0899	Technical Library	9536	(electronic copy)


Sandia National Laboratories